Pandal-Blanco, A.; Payri, R.; García-Oliver, JM.; Pastor Enguídanos, JM. (2017). Optimization of spray break-up CFD simulations by combining Sigma-Y Eulerian atomization model with a response surface methodology under diesel engine-like conditions (ECN Spray A). Computers & Fluids. 156:9-20. doi:10.1016/j.compfluid.2017.06.022

Optimization of spray break-up CFD simulations by combining **Σ**-Y Eulerian Atomization Model with a Response Surface Methodology under diesel engine-like conditions (ECN spray A)

A. Pandal[a,*], R. Payri[b], J.M. García-Oliver[b], J.M. Pastor[b]

[a] *Departamento de Energía (Área de Mecánica de Fluidos), Universidad de Oviedo, Spain*
[b] *CMT-Motores Térmicos, Universitat Politècnica de València, Spain*

Abstract

This work evaluates the performance of the Σ-Y Eulerian atomization model at reproducing the internal structure of a diesel spray with a special focus on Sauter Mean Diameter (SMD) predictions. Modeling results have been compared to x-ray radiography measurements [21, 24, 38] which provided unique data within dense spray region. The first step corresponds to accurately reproduce the large scale spray dispersion. Among different RANS turbulence models, the standard k-ε with the round jet corrected $C_{1\epsilon}$ value (1.60), has shown the best performance, as shown in [12] . Then, the study is devoted to the application and optimization of the predicted interphase surface density (Σ). In this work, a combination of CFD modeling and the statistical Design of Experiments (DOE) technique known as Response Surface Method (RSM) is applied in order to improve Sauter Mean Diameter (SMD) predictions from Σ equation compared to experimental measurements. In

*Corresponding author
Email address: pandaladrian@uniovi.es (A. Pandal)

the investigation, two different optimizations are conducted for the three modeling parameters involved in the equation, following a Central Composite Design (CCD), leading to 15 simulations for each one. After that, both optimum sets of values are validated to assure the accuracy of the method and it is decided the best choice. Finally, different injection and ambient conditions are simulated, with those selected values, providing a remarkable improvement in the modeling performance.
Keywords: Eulerian, Diesel spray, Near-field, SMD, CFD, Response surface method

1. Introduction

Recent investigations of modern diesel engines are highly focused on achieving both high efficiency and reduced emissions, due to more restrictive regulations, the cost of diesel fuel and the increasing global environmental concern of population. This goal is tightly related to the fuel injection process and the subsequent fuel-air mixing, which depends on the injector characteristics and nozzle geometry [33, 34, 35, 36]. Therefore, an accurate prediction of these processes is required in order to produce reliable engine performance and emissions predictions.

In spite of the great practical interest in how sprays emanate from fuel injectors, the dense spray region just outside of fuel injectors has remained a challenge for both experimentalists and spray modelers. This near-field of the spray is a optically dense space at which only special diagnostics such as x-ray radiography [21, 23, 24, 38] can obtain reliable data.

From the modeling side, classical approaches carried out by means of

the Discrete Droplet Method (DDM) [15], although commonly used in spray simulation studies [2, 26, 27, 37, 57], are not necessarily appropriate from a physical point of view for describing the near nozzle region of the spray. This method is well-suited for low liquid volume fraction flows and the majority of existing drag, collision, breakup, and vaporization models are based on assumptions of near-spherical droplets in a sparse spray. Instead of this type of models, recent Eulerian modeling have shown great promise [3, 7, 12, 18, 25, 43, 52, 54, 56]. In this kind of model, an Eulerian description is applied to solve the two-phase flow assuming both liquid and gas phases as continuum. These models emphasizes the turbulent mixing of the gas and liquid, which is consistent with the observations of Siebers [44, 45, 46], based on numerous experiments, that 'the processes of atomization and the ensuing interphase transport of mass and energy at droplet surfaces are not limiting steps with respect to fuel vaporization in DI diesel sprays'. So Eulerian treatments of the dense spray seem to have physical advantages. In order to account for small-scale atomization, a diffusive interface approach is applied for high Reynolds and Weber number present in Diesel sprays [51]. The interphase is then modeled by a surface density (Σ) equation, defined as the liquid-gas interface area per unit volume.

One of the most challenging topics of these Eulerian CFD modeling of diesel sprays, is precisely the calibration of the surface density equation. This procedure can be made in terms of numerical comparison with CFD direct numerical simulation (DNS) results [11, 25, 32] or from a more practical point of view, by comparison with experimental measurement of SMD [51, 4, 54, 5]. This last methodology, although extremely interesting, lacked on

the sufficient data on the near-field (downstream distance $\frac{x}{d} < 100$) of diesel sprays, until now [21]. Independently of the chosen method, to the author's knowledge the study of different values for the modeling constants is made by means of a nearly arbitrary selection. In the present work, a statistical Design of Experiments (DoE) technique known as Response Surface Method (RSM) is used in order to obtain an optimum set of modelling constants.

The design of experiments (DoE) methodology has been applied to different knowledge fields [1, 6, 19, 47], because of its high reliability and accuracy in the results. The other great advantage of this statistical analysis is the huge reduction in the number of simulations needed to achieve the optimum set of values for the input parameters, which predefine exactly the number of iterations, in comparison with evolutive methods in which the number of iterations is unknown forehand since the termination point is arbitrary in order to assure not obtaining a local optimum. Finally, an important outcome from these studies, apart from the optimum configuration, is the gained knowledge about mutual effects between the variables and their individual effect on the final results.

In the present research work, a fully Eulerian Σ-Y model [18], implemented in the OpenFOAM CFD open source c++ library [55], is evaluated to simulate diesel engine-like conditions against experimental measurements available from the database of the Engine Combustion Network (ECN) [16]. In first term, the investigation is focused on the correct prediction of the diesel spray structure in the near-nozzle region. Different turbulence models are evaluated in order to achieve the best configuration in comparison with experimental measurements, of both in-nozzle and external flow variables.

After that, once the large scale flow features are well captured, a statistical methodology for optimizing the predictions of the mean size of liquid fragments, based on the RSM approach, is applied. The optimization process carried out, uses 3 inputs (modeling constants), which results in a test plan of 15 simulations. Considering these results, a set of optimum values for the modeling constants can be obtained, whose SMD predictions are finally evaluated in comparison with the ones provided by the original (reference) set of constants for different ambient and pressure injection conditions. The aim of the paper is to evaluate the capabilities of the Σ-Y Eulerian model to accurately predict both the liquid dispersion and atomization of a diesel spray and to determine the proper values for interphase surface density modeling constants in these sprays.

2. Σ-Y model description

The Σ-Y model considers the liquid/gas mixture as a pseudo-fluid with a single velocity field. Under the assumption that the flow exiting the injector is operating at large Reynolds and Weber numbers, it is possible to assume a separation of the large scale flow features, such as mass transport, from the atomization process occurring at smaller scales. This allows the direct simulation of the large scale bulk transport of the liquid while unresolved turbulent transport is modeled using standard closures such as those used in Reynolds-averaged turbulence models.

To track the dispersion of the liquid phase an indicator function is used, taking a value of unity in the liquid phase and zero in the gas phase. The mean liquid volume fraction is denoted ($\overline{Y}$) and the mean mass averaged fraction is defined as ($\tilde{Y} = \frac{\overline{\rho Y}}{\bar{\rho}}$). Favre averaging the transport equation for

the liquid mass fraction yields Eq. (1)

$$\frac{\partial \bar{\rho}\tilde{Y}}{\partial t} + \frac{\partial \bar{\rho}\tilde{u}_i\tilde{Y}}{\partial x_i} = -\frac{\partial \bar{\rho}\widetilde{u'_i Y'}}{\partial x_i} \tag{1}$$

where u' denotes the density weighted turbulent fluctuations in velocity and Y' denotes turbulent fluctuations in liquid mass fraction. The turbulent diffusion liquid flux term, $\widetilde{u'_i Y'}$, captures the effect of the relative velocity between the two phases [51]. This term is modeled using a standard turbulent gradient flux model, which law successfully worked for Diesel spray compared to DNS results, as indicated in [11].

$$\bar{\rho}\widetilde{u'_i Y'} = -\frac{\mu_t}{Sc}\frac{\partial \tilde{Y}}{\partial x_i} \tag{2}$$

where μ_t is the turbulent viscosity and Sc is the Schmidt number.

While the approach used here assumes that the resolved momentum of the liquid/gas mixture can be characterized by a single bulk velocity, the slip velocity can be expressed explicitly as derived by [10] and seen in Eq. (3).

$$u_i|_l - u_i|_g = \frac{1}{\tilde{Y}\left(1-\tilde{Y}\right)} \cdot \widetilde{u'_i Y'} \tag{3}$$

The following momentum equation is used:

$$\frac{\partial \bar{\rho}\tilde{u}_j}{\partial t} + \frac{\partial \bar{\rho}\tilde{u}_i\tilde{u}_j}{\partial x_i} + \frac{\partial}{\partial x_i}\left(\bar{\rho}\widetilde{u'_i u'_j} - \mu\frac{\partial \tilde{u}_j}{\partial x_i}\right) = -\frac{\partial \tilde{p}}{\partial x_j} \tag{4}$$

In this equation, the third term on the left-hand side (LHS) is the corresponding to the Reynolds stresses ($\bar{\rho}\widetilde{u'_i u'_j}$) collected with the viscous normal and shear stress terms ($\mu\frac{\partial \tilde{u}_j}{\partial x_i}$). The closure corresponding to these Reynolds stresses is given by different two equation turbulence models, which performance is evaluated (see Section 6.1).

Under the assumption that the two phases form an immiscible mixture, the mass-averaged value of the indicator function is related to the density by:

$$\frac{1}{\bar{\rho}} = \frac{\tilde{Y}}{\rho_l} + \frac{1-\tilde{Y}}{\rho_g} \tag{5}$$

An equation of state is then assigned to each phase. The gas phase obeys an ideal gas law, while the liquid phase is estimated following the Hankinson-Brobst-Thomson (HBT) correlation [40], in which the liquid density is a function of temperature (T) and pressure (p).

To close the above system of equations, the temperature is obtained from a bulk mixture enthalpy equation expressed in the following terms:

$$h\left(T\right) = \tilde{Y} \cdot h_l\left(T\right) + \left(1-\tilde{Y}\right) \cdot h_g\left(T\right) \tag{6}$$

Here h_l and h_g denote the enthalpy of the liquid and gas phases respectively, and are calculated as the integrals of

$$dh_l = c_{p,l} dT \tag{7}$$

$$dh_g = c_{p,g} dT \tag{8}$$

where $c_{p,i}$ is the specific heat capacity at constant pressure. This is obtained as a function of temperature T from a set of coefficients taken from JANAF tables of thermodynamics. For the liquid phase, then it is applied the Rowlinson-Bondi equation [40].

Finally, being h the static enthalpy implemented through the following conservation equation, where α_{eff} is the effective turbulent thermal diffusivity and $\tau_{ij}\frac{\partial u_j}{\partial x_i}$ the viscous dissipation, being τ_{ij} the viscous stress tensor from

the turbulence model:

$$\frac{\partial \bar{\rho} h}{\partial t} + \frac{\partial \bar{\rho} \tilde{u}_i h}{\partial x_i} - \frac{\partial}{\partial x_i}\left(\alpha_{eff} \frac{\partial h}{\partial x_i}\right) = \frac{\partial p}{\partial t} + u_i \frac{\partial p}{\partial x_i} + \tau_{ij} \frac{\partial u_j}{\partial x_i} \tag{9}$$

The solution of the above equations fully characterizes the large-scale bulk motion of the flow. Several other options exist for obtaining closure in the above system of equations (see for example the discussion in [10] and [49]).

Conversely, the small scale atomization is modeled by solving a transport equation for the evolution of the interphase surface area density Σ. This surface density can be understood as the amount of spatial surface per unit volume at a given time and spatial position. It is not easy to establish even an unclosed form of the balance equation of this quantity. Ishii [20] and Delhaye et al.[9] made some attempts on two phase flow applications and by means of the spatial averaging operator, the averaged surface density equation is introduced by Ishii [20] in a similar form to the development of flame surface area density [8, 29] used in combustion applications. Then, Ishii's original equation was adopted by Vallet and Borghi [50], in which nearly all the models in the literature are based, and gives the following evolution equation for this quantity, assuming a gradient law closure for the turbulent diffusion flux term, where D_Σ is a suitable diffusion coefficient usually taken as the turbulent kinematic viscosity (ν_t) over a Schmidt number (Sc_Σ) and $S_{\Sigma_{init}}$ is a proper initialization term.

$$\frac{\partial \tilde{\Sigma}}{\partial t} + \frac{\partial \tilde{u}_j \tilde{\Sigma}}{\partial x_j} - \frac{\partial}{\partial x_j}\left(D_\Sigma \frac{\partial \tilde{\Sigma}}{\partial x_j}\right) - a\tilde{\Sigma} + b\tilde{\Sigma}^2 - S_{\Sigma_{init}} = 0 \tag{10}$$

where the inverse time-scale a and coefficient b can be understood as the sur-

face generation due to the growth of fluid instabilities (i.e. Kelvin-Helmholtz) and the destruction of surface due to droplet coalescence (in the case of dispersed flow), respectively. However, the most common form for the combination of these two source terms is the restoration to an equilibrium value ($\bar{\Sigma}_{eq}$) [4, 51]:

$$\frac{\partial \tilde{\Sigma}}{\partial t} + \frac{\partial \tilde{u}_j \tilde{\Sigma}}{\partial x_j} - \frac{\partial}{\partial x_j}\left(D_\Sigma \frac{\partial \tilde{\Sigma}}{\partial x_j}\right) - C_\Sigma \tilde{\Sigma}\left(1 - \frac{\tilde{\Sigma}}{\bar{\Sigma}_{eq}}\right) - S_{\Sigma_{init}} = 0 \tag{11}$$

The $\bar{\Sigma}_{eq}$, already mentioned, is the equilibrium or critical surface density to which the local surface density is driven and it is set by a suitable equilibrium droplet radius (r_{eq}):

$$\bar{\Sigma}_{eq} = \frac{3\bar{\rho}\tilde{Y}}{\rho_l r_{eq}} \tag{12}$$

As proposed by Vallet et al. [51] assuming that droplet collision is the principal mechanism in the droplet breakup the equilibrium radius can be derived:

$$r_{eq} = \alpha_2 \frac{\sigma^{3/5} l_t^{2/5}}{\tilde{k}^{3/5}} \frac{(\bar{\rho}\tilde{Y})^{2/15}}{\rho_l^{11/15}} \tag{13}$$

where σ is the surface tension, l_t the turbulent length scale and $\tilde{k}$ the turbulent kinetic energy. Then, the coefficient C_Σ is modeled as the inverse of the turbulent time scale, where $\tilde{\varepsilon}$ is the turbulent dissipation:

$$C_\Sigma = \alpha_1 \frac{\tilde{\varepsilon}}{\tilde{k}} \tag{14}$$

note the presence of two modeling constants (α_1, α_2), which by default are equal to 1 [51], although other values have been evaluated [4, 5, 51, 54].

Finally, as can be seen all the source terms that are involved in this equation are proportional to the interface surface density Σ. As a result, there will be no production if there is no interface. This is solved by means of the already mentioned initialization term $S_{\Sigma_{init}}$. For that purpose, a minimum value of Σ is considered in any computational cell which is not filled with pure liquid or gas. In a similar way as in Wang et al. [53], this minimum value is estimated as $V^{-1/3}$ where V is the volume of the CFD cell. The source term only takes a positive value if the interface field is lower than this Σ_{min}:

$$S_{\Sigma_{init}} = \frac{\Sigma_{min} - \Sigma}{\Delta t} pos(\Sigma_{min} - \Sigma) \tag{15}$$

where pos is a boolean pre-implemented operator in OpenFOAM:

$$pos(x) = \begin{cases} 1 & \text{if } x > 0 \\ 0 & \text{if } x \leq 0 \end{cases}$$

Together with the mass averaged liquid fraction, the interphase surface area density can be used to derive results for droplet sizing, such as the local SMD (D_{32}) of the spray and the drop number density.

$$D_{32} = \frac{6\bar{\rho}\tilde{Y}}{\rho_l \tilde{\Sigma}} \tag{16}$$

$$n = \frac{\rho_l^2 \bar{\Sigma}^3}{36\pi \bar{\rho}^2 \tilde{Y}^2} \tag{17}$$

A further description of the numerical implementation of this solver can be found in [18].

3. Experimental data

In order to evaluate and validate the model applied to spray simulations, the ECN Spray A database [16, 17, 22, 21] has been used. The "Spray A" condition consists of a free diesel spray injected into a quiescent environment, where well-defined boundary conditions and experimental data are available for model validation purposes. The nominal condition for Spray A corresponds to 150 MPa injection pressure, 900 K ambient temperature and 22.8 kg/m^3 as ambient density.

In this case, the Spray A non-evaporating condition of ECN is used in order to evaluate the model in terms of the near-field structure (dense region) of diesel sprays, taking advantage of the valuable x-ray radiography measurements available at ECN database. This experiment is conducted with the ambient gas at room temperature (303 K) due to the x-ray transparent polymer windows used, which cannot be used at high temperature. Nevertheless, the same ambient density of the nominal evaporating Spray A condition is matched in order to reproduce similar conditions for the spray breakup process, assuming that density is a more critical parameter than pressure for atomization [31]. The main conditions of this experiment are presented in Table 1. Further details about the experimental set-up are provided in [24].

The experimental data used for validation include the projected mass density (PMD) of the fuel, which is calculated by a line-of-sight integration along the x-ray beam [24, 38], see Equation 18 and Figure 1. Another useful quantity obtained from the x-ray radiography measurements is the transverse integrated mass (TIM), which is obtained from the integral of the projected density across the transverse position at a particular axial location

Table 1: Conditions for non-evaporating Spray A experiment

Fuel	n-Dodecane
Ambient composition	100% N2
Injection pressure [MPa]	150
Ambient temperature [K]	303
Ambient density [kg/m^3]	22.8
Fuel injection temperature [K]	343

Table 2: Simulated cases conditions, including injection pressure, ambient temperature and back pressure- USAXS measurements

Injector Serial#	P_{inj} [MPa]	T_{amb} [K]	P_{amb} [MPa]
210675 (Baseline)	150	303	2.0
	Ambient Conditions	Study	
210675	150	303	0.67
	Injection Pressure	Studies	
210675	100	303	2.0
210675	50	303	2.0

[23]. Moreover, liquid volume fraction can be evaluated. This measurements are made by a tomography reconstruction of radiography data for liquid volume fraction [38]. Finally, the characterization of the large scale of the flow is completed by means of a typical global spray parameter such as penetration. Additionally, measurements of droplet size made using ultra-small angle x-ray scattering (USAXS) technique [21], have been used in order to calibrate the Σ model constants to accurate predict droplet sizes. These measurements are available for different injection pressures and ambient conditions, see Table 2.

$$PMD(x,r) = \int \rho_l(z), dz \tag{18}$$

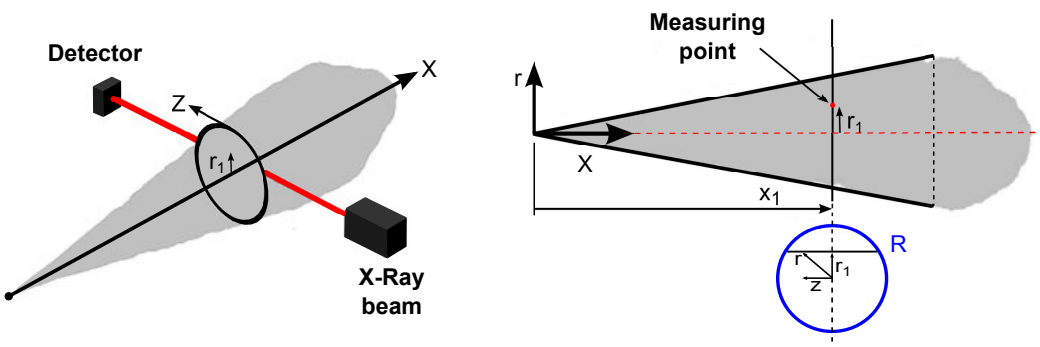

Figure 1: Scheme of x-ray measurement technique and description of integration for calculating the projected mass density. Figure adapted from Desantes et al.[14]

Table 3: Nozzle geometric characteristics for single-hole Spray A ECN injector. D_o, D_i, L and r denote nozzle orifice outlet diameter, nozzle orifice inlet diameter, length, and inlet radius, respectively

Injector Serial#	$D_o[\mu m]$	$D_i[\mu m]$	L/D_o[-]	r/D_o[-]	k-factor	exit offset $[\mu m]$
210675	89.4	116	11.5	0.23	2.7	53

Detailed internal nozzle geometric characterization has been performed for the injector employed in these experiments, where the main characteristics are presented in Table 3. D_o, D_i, L and r denote nozzle orifice outlet diameter, nozzle orifice inlet diameter, length, and inlet radius, respectively. The nozzle convergence is described by the k-factor, as defined in [28].

4. Computational Domain and Model set-up

In order to conduct this study, some of the conclusions presented by Desantes et al. [13] will be used as initial set-up. Nozzle geometric parameters have a great influence on the spray behavior. Thus, including nozzle effects by coupling internal and external flow simulations leads to a better representation of reality. In [13] was shown that internal and external flow

calculations can be performed independently, which permits to feed the inlet boundary condition of an external flow simulation with the fields obtained at the nozzle exit in a coupled internal/external flow study. This is a key conclusion because several calculations have to be made due to the use of an statistical method. Thus, being able to simulate an accurate and reliable spray behaviour by only an external flow saves an enormous amount of calculation time.

Additionally, in Desantes et al. work [13] was shown that both 3D and 2D simulations produced qualitatively and quantitatively good results with an important computational cost reduction in the case of the 2D computational domain (see Table 4), thus only 2D simulations are chosen for this work.

Table 4: Computational cost comparison between different simulations

Simulation type	Wall clock time (hours)	Number of CPU
3D coupled	936	24
2D coupled	72	12
2D decoupled	56	12

Two different 2D axisymmetric computational domains are used. First of all, a mesh including the nozzle geometry is considered together with a spray chamber of 12 mm in length and 14 mm in diameter. In Fig. 2a, the mesh structure can also be seen. It consists of 89000 cells with 72 elements at the orifice exit, presenting a minimum cell size of 1.5 μm near the walls inside the nozzle and a maximum cell size of 250 μm far from the orifice exit [13].

Finally, in order to simulate a fully developed spray with the Σ-Y Eulerian model, a 2D axisymmetric computational domain without the nozzle geometry is considered. The mesh is structured with non-uniform grid resolution.

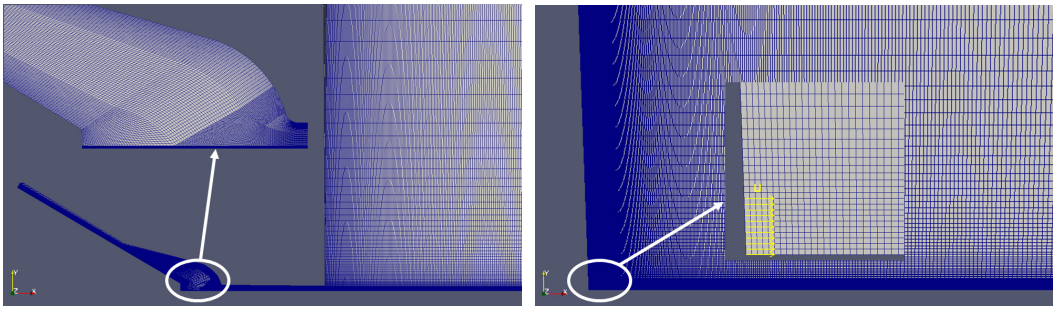

(a) Grid used for coupled nozzle-spray simulations

(b) Grid used for de-coupled spray simulations

Figure 2: Computational grids for Spray A simulations

There are 20 cells along the orifice diameter, keeping an aspect ratio close to one in the near nozzle region, as depicted in Fig. 2b. The non-uniform grid resolution consists of cells with an expansion ratio of 1.01 and 1.06 in the axial and radial directions, respectively, as indicated in [18]. Note that all the computational domains use the axis orientation convention from Kastengren et al. [22].

Boundary conditions selected for all the walls of the domains are no-slip. A non-reflexive boundary condition is used for the outlet and a time varying velocity condition is used for the inlet. In the case of the coupled simulation, the inlet velocity is obtained from experimental mass flow measurements [22], domain inlet area and fuel density. A uniform velocity distribution at the domain inlet is assumed. This inlet condition was used instead of a constant pressure profile because this would not capture the experimentally observed time oscillations in the flow. This is because these oscillations are highly influenced by the transient needle movement profile, and these simulations used a static mesh with the needle positioned at maximum lift. From the

external flow simulations side, as previously discussed, the fields obtained at the nozzle exit in the coupled simulation were used as inlet boundary condition. To do that, the mapped boundary condition of OpenFOAM is used. Moreover, the discretization of the divergence terms was solved with a Gamma NVD scheme, and a first order Euler scheme is applied for time derivative terms.

5. Methodology

The first step of the procedure consists on modeling accurately the structure of the diesel spray in the near-nozzle region. Thus, the coupled computational domain is used, and different turbulence models are evaluated in order to achieve the best possible match with measurements, both in-nozzle and external flow variables. The assessment of the turbulence models is completed with independence of the modeling calibration conducted for the small scale atomization, this is possible thanks to the separation hypothesis (large versus small scales) of the Σ-Y model. Once the liquid dispersion is correctly captured, in a second stage, the optimization of the interphase surface density equation predictions, based on SMD measurements, is made. The methodology for this optimization is based on Design of Experiments (DOE) techniques, particularly the Response Surface Method (RSM). This method was selected to calibrate the constants that appear at the phenomenological source/sink terms of the surface density model equation. Apart from providing an optimum set of values, it can reveal valuable information about the cause/effect relations between the input and the output parameters.

In these calibration studies three parameters from Eq.(11) are chosen to be optimized (modeling constants α_1, α_2 and Sc_Σ), and a Central Compos-

ite Design (CCD) [30] defined the DOE test plan with 15 simulations, all conducted using the 2D decoupled simulation, i.e. using as inlet boundary condition the nozzle exit profiles obtained with a coupled simulation. The optimization is done based on the path-averaged SMD [21] and specifically, the output parameter of RSM is the mean error between the measurements along the axis and the calculated SMD, which is computed at a time late enough to ensure quasi-steady state predictions. Thus, as explained in[21], the provided experimental SMD is likewise pathlength-integrated because both the scattering and radiography measurements are pathlength-integrated. As a result, model predictions are processed following the path-averaged ECN method. The SMD of droplets within each CFD cell is integrated through the depth of the spray, collapsing the SMD to a 2-D map (it should be noted that for 2D computations, axisymmetry is assumed).

6. Results and Discussion

6.1. Nozzle and spray flow – Effect of turbulence models

The standard k-ε turbulence model with the round-jet corrected $C_{1\epsilon}$ value (1.60)[39], which was successfully used for internal [13, 56] and external [18] diesel spray simulations, was evaluated together with the SST k-ω and the RNG k-ε turbulence models. These additional models are commonly used for internal nozzle flow simulations in literature [41, 42, 43, 48] and thus, it is worthy to investigate their modeling performance.

Firstly, momentum and mass fluxes are evaluated at the nozzle exit from the different CFD calculations. Then, non-dimensional flow coefficients are calculated from such results to define the performance of the turbulence model under such conditions.

Table 5: Steady state parameters (mass flow rate-$\dot{m}$ and momentum-$\dot{M}$) and non-dimensional flow coefficients for the turbulence models tested (velocity coefficient-Cv, area coefficient-Ca and discharge coefficient-Cd)

Turbulence model	$\dot{m}$(g/s)	$\dot{M}$(N)	Cv[-]	Ca[-]	Cd[-]
Experimental	2.558	1.52	0.918	0.98	0.9
Std k-ε	2.54	1.477	0.903	0.976	0.881
RNG k-ε	2.536	1.472	0.9	0.977	0.879
SST k-ω	2.546	1.465	0.893	0.99	0.884

Table 5, shows the steady state values of momentum and mass fluxes as well as the dimensionless coefficients simulated, compared to experimental ones. These flow coefficients are the discharge coefficient, C_d, the most important one.

$$C_d = \frac{\dot{m}_f}{\dot{m}_{f,th}} = \frac{\dot{m}_f}{A_0\sqrt{2\rho_f \Delta p}}$$

where $\dot{m}_f$ is the mass flow, Δp is the difference between the injection pressure (P_{inj}) and the back pressure (P_{amb}), A_0 is the geometrical area of the outlet of the orifice and ρ_f is the liquid fuel density. The second parameter is the velocity coefficient, C_v, which is defined as the effective velocity divided by the maximum Bernoulli's theoretical velocity, u_{th}.

$$u_{th} = \sqrt{\frac{2\Delta p}{\rho_f}}$$

And the last non-dimensional flow parameter is the area coefficient, C_a, which is defined as the effective area divided by the geometrical area. Using the momentum flux in combination with mass flow predictions, the effective injection velocity and effective injection area can be calculated

$$u_{eff} = \frac{\dot{M}}{\dot{m}_f}$$

$$A_{eff} = \frac{\dot{m}_f^2}{\rho_f \ \dot{M}}$$

and then, the dimensionless coefficients:

$$C_d = C_a \ C_v = \frac{A_{eff}}{A_0} \ \frac{u_{eff}}{u_{th}}$$

At the sight of the results, no large differences could be detected among the different turbulence models tested, with maximum deviations compared to the Std k-ε model below 1.5%. The SST k-ω model is consistently showing the largest deviations, both to the other models as well as to experimental values as well as the largest area coefficient, due to it presents stepper profiles close to the walls at the nozzle exit, see Fig. 3. Moreover, the three models predict values with an error lower than 5% with respect to experimental ones. Such results prove that Std k-ε model performance for in-nozzle simulations is as good as the one provided by the other two more typically used turbulence models.

In order to draw a more accurate conclusion about turbulence model performance, near nozzle spray predictions should be investigated. The projected mass density of the fuel, as explained before, is used for validation. In order to enable fair comparisons of simulated predictions against experiments, a similar calculation procedure (line-of-sight integration along the x-ray beam[24, 38]) is replicated with the CFD data. The model predicted results of projected mass density with these three turbulence models are compared against x-ray radiography measurements in Fig. 4. From these pro-

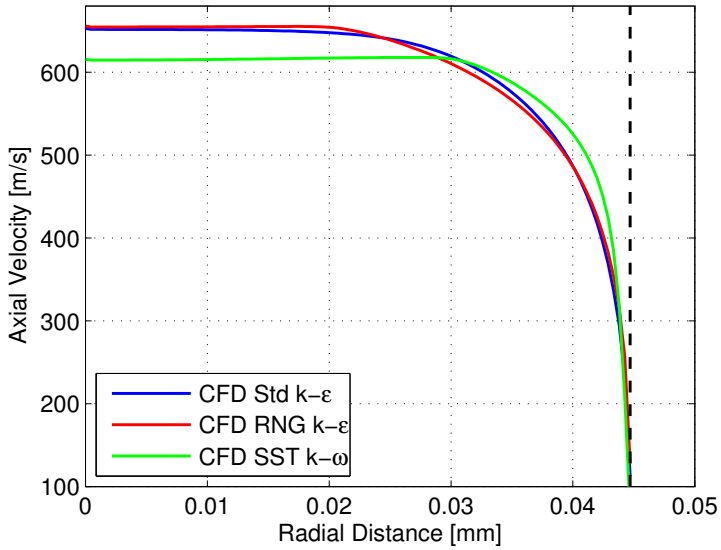

Figure 3: Computed axial velocity profiles at 500 μs after SOI at the orifice exit for 2D CFD coupled simulations with different turbulence models. Black dashed line depicts the radius of the nozzle orifice

jected density contours, large differences can be observed among the three simulations. While predictions achieved with the Std k-ε model can capture the fuel distribution in the very near-nozzle region, as shown in Desantes et al. [13], simulations using the other two turbulence models over-predict the radial dispersion downstream 2 mm. This indicates that these two turbulence models are too diffusive for external spray modeling in this case.

Additionally, the projected density along the transverse direction comparing the simulations and x-ray radiography data is shown at 0.1 mm, 2 mm, and 6 mm downstream of the nozzle exit in Fig. 5. At the first location all the models predicts almost the same profiles and no noticeable differences could be detected among them, in agreement to very similar flow coefficients previously discussed. However, predictions at 2 mm downstream of the nozzle

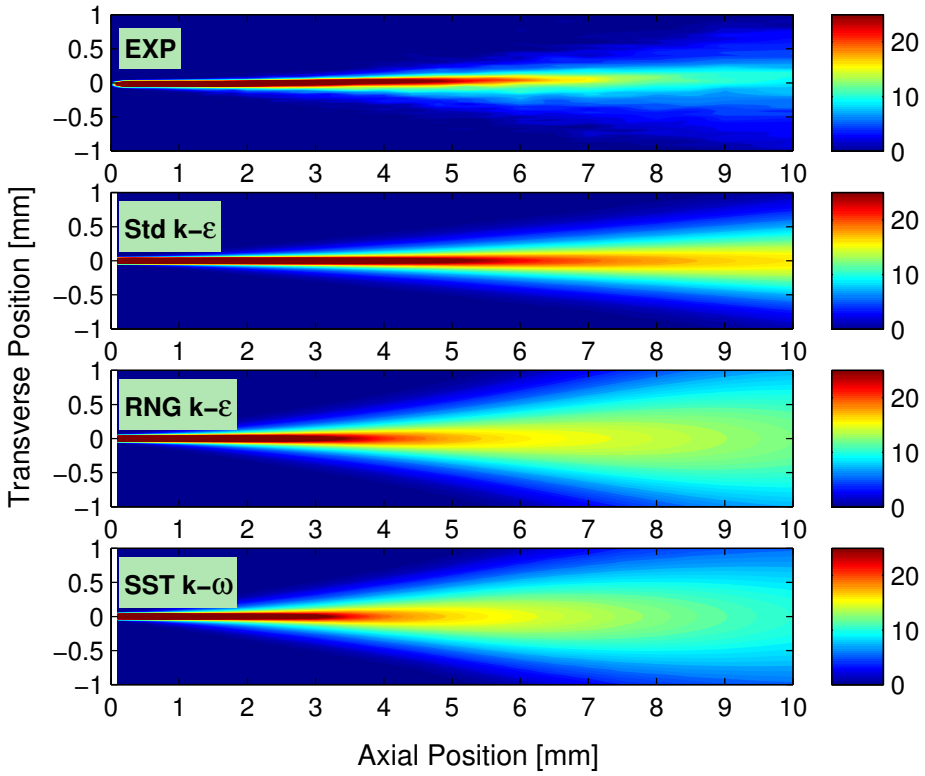

Figure 4: Projected mass density distributions [μg/mm^2] at 500 μs after SOI from x-ray data and baseline 2D CFD coupled simulations for different turbulence models

exit show significant contrast. Projected mass density predictions by both the RNG k-ε and SST k-ω turbulence models are under-predicting experimental values, in terms of peak value, and over-predicting experimental values in terms of radial dispersion. At 6 mm downstream, the same conclusions hold, with even more important differences to the measurements.

TIM, transverse integrated mass, which is obtained from the integral of the projected density across the transverse position at a particular axial location[23], is also evaluated by another integration of the CFD projected mass density predictions. This is used to compare the TIM profile along the

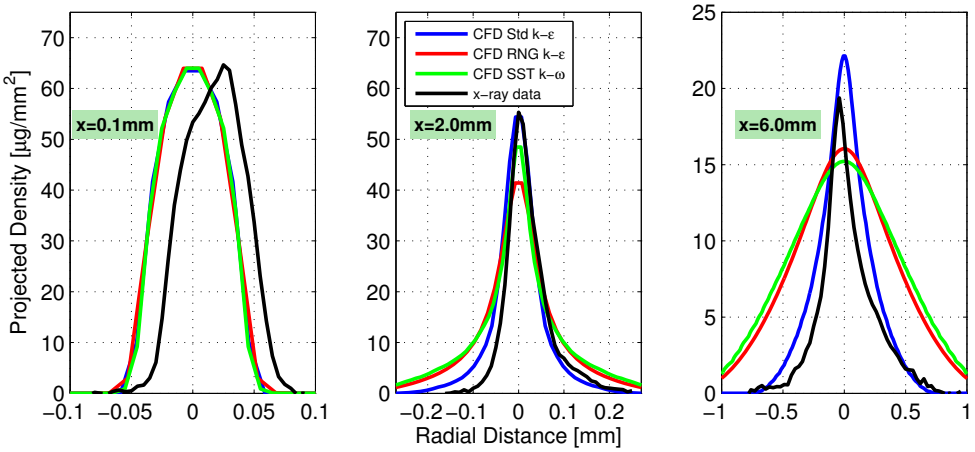

Figure 5: Computed (blue-Std k-ε, red-RNG k-ε and green-SST k-ω) and measured (black lines) profiles of projected mass density [μg/mm^2] at 500 μs after SOI at axial locations of 0.1 mm, 2 mm, and 6 mm downstream of the nozzle exit for 2D CFD coupled simulations with different turbulence models

axis among the simulations and x-ray data. Figure 6 shows the predicted results of simulations, using the three different turbulence models, compared with measurements. As expected in light of the previous results, this figure shows that TIM rises faster in these simulations due to an inadequately fast spray mixing.

These simulations make it clear that the Std k-ε turbulence model provides the best match with the experimental data for the external flow and in the near-field, where it can capture the trend of the internal structure of a diesel spray, while keeping a fair performance regarding the nozzle flow (i.e. in terms of non-dimensional coefficients) in the range of other RANS models.

However, these coupled internal/external flow simulations present a high computational cost and as presented in [13]. It was also shown in this work that there are not great differences between the coupled internal/external flow simulation and the decoupled one, in which only the external flow is

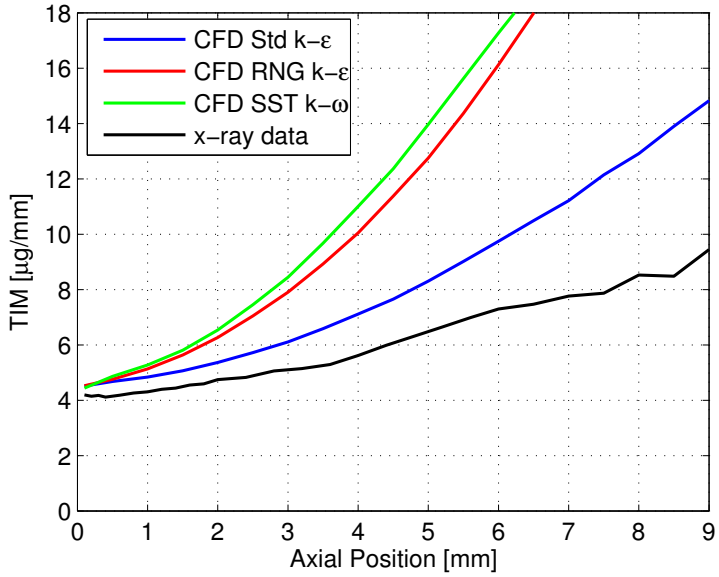

Figure 6: Computed (blue-Std k-ε, red-RNG k-ε and green-SST k-ω) and measured (black lines) transverse integrated mass along the axis at 500 μs after SOI for 2D CFD coupled simulations with different turbulence models

simulated (by feeding the inlet boundary condition with the fields obtained at the nozzle exit in a coupled internal/external flow study). As a result, decoupled simulation is used for the following studies together with the Std k-ε turbulence model. In order to finally assure a good prediction of the large scale flow, typical global spray parameters such as penetration and also the liquid volume fraction (LVF) field are evaluated, to check effects on the spray tip penetration evolution, spray dispersion and the intact core length. In Fig. 7 spray penetration (left) and predicted centerline liquid volume fraction profiles (right) are compared. In terms of spray penetration, predictions achieved by the simulation match with great accuracy the experimental measurements falling within the uncertainty of measurements. In terms of profiles of liquid volume fraction on the axis, it must be noted that

experimental measurements are available only within the first 12 mm. This measurements, available at [17], are made by a tomography reconstruction of radiography data for liquid volume fraction [38]. The simulation performance is quite remarkable, being able to match exactly the decay of the liquid volume fraction and predicting an intact liquid core ($LVF > 0.9$) almost in the range estimated by recent analyses in [38]. Both variables are reasonably predicted showing the effectiveness of capturing the effects of the internal nozzle flow in the near nozzle region of the spray.

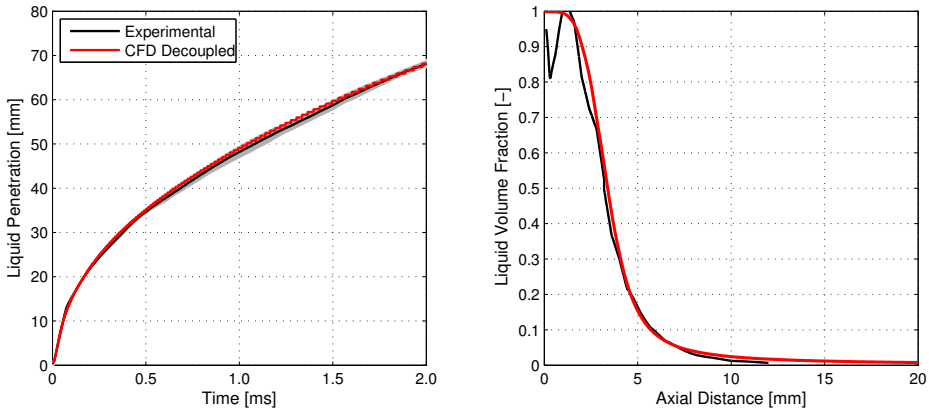

Figure 7: Spray penetration [left] and computed centerline liquid volume fraction at 1 ms after SOI [right] for decoupled simulation. CFD predictions-red line and experimental measurements-black line

6.2. Spray break-up

Droplet size measurements made using the ultra-small angle x-ray scattering (USAXS) technique [21], have been used in order to calibrate the Σ model constants. These measurements were made for different injector nozzles, two spray A nozzles (single hole) and one spray B nozzle (3-hole). Nevertheless, the wide range of operating conditions (see Table 2) are only

available for injector nozzle serial # 210675 and due to that, only this nozzle is used in the present work.

An example of main features of USAXS SMD data are presented in Figure 8. There is a rapid decrease near the nozzle followed by a region where SMD gets more stable. In general, SMD reaches a minimum and tends to slightly increase with axial distance. Those trends could also be observed in CFD predictions using the default calibration constants (see Table 6), but SMD levels are under-predicted. Note that SMD model predictions are only considered downstream of the intact liquid core ($LVF > 0.9$), i.e. from $2.5mm$ as seen in Fig. 7

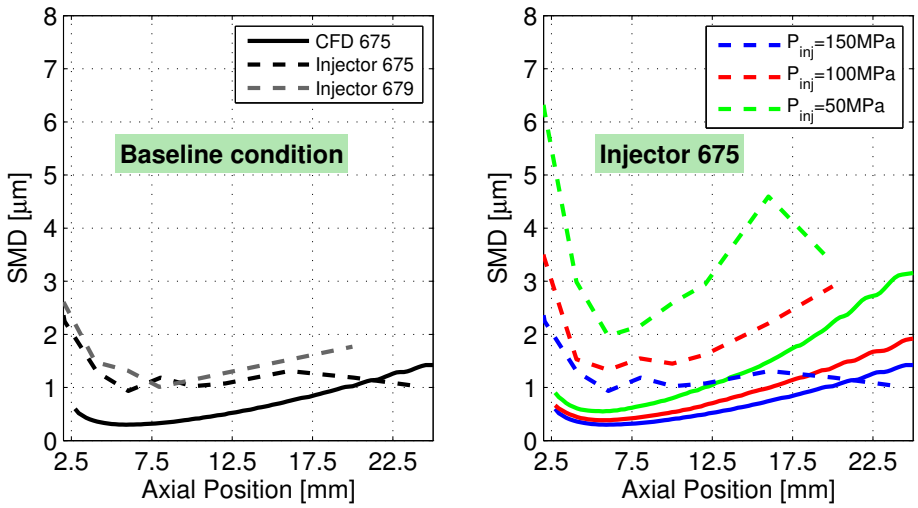

Figure 8: Measured (dashed lines) and reference CFD predicted SMD (solid lines) for the baseline condition [left] and for different injection pressures [right]

In a first step, the optimization was made for the spray A baseline condition ($P_{inj} = 150\ MPa$), named as optimization at high pressure injection (HP), but for this operation point experimental results show a particular trend. In contrast to the general thought and the other injection pres-

sures (medium and low) cases measured, the axial evolution of SMD shows a steadily decreasing trend with axial position, with no further increase due to coalescence, which might be expected under this operating condition. As shown in Figure 8 it is also remarkable that for other spray A injector (serial # 210679), for the baseline condition, the SMD growing with axial position is more noticeable [21]. For this reason, it is decided to conduct two different optimizations. Thus, additionally to the baseline condition, another optimization for the intermediate injection pressure case ($P_{inj} = 100\ MPa$) is made, optimization at medium pressure injection (MP).

At the end of the process, both optimum sets of model constants values obtained from the response surface are validated for the corresponding operating condition to assure the accuracy of the method and the modeling performance improvement with respect to the original one (Reference in Table 6). Then, it is decided the best choice of modeling parameter values and afterwards, the different injection pressure conditions and the ambient study (see Table 2) are simulated with those optimum constants and compared against the experimental measurements in order to finally check the overall validity of the chosen modeling parameter values.

6.2.1. Optimization stage

Following the explained methodology, now the statistical optimization of the interphase surface density modeling parameters is conducted by means of the DOE technique known as Response Surface Method.

Concerning the input factors, the default values of the three modeling constants of the interphase surface density equation are selected at the reference point, while in order to define the parameter ranges of the DOE,

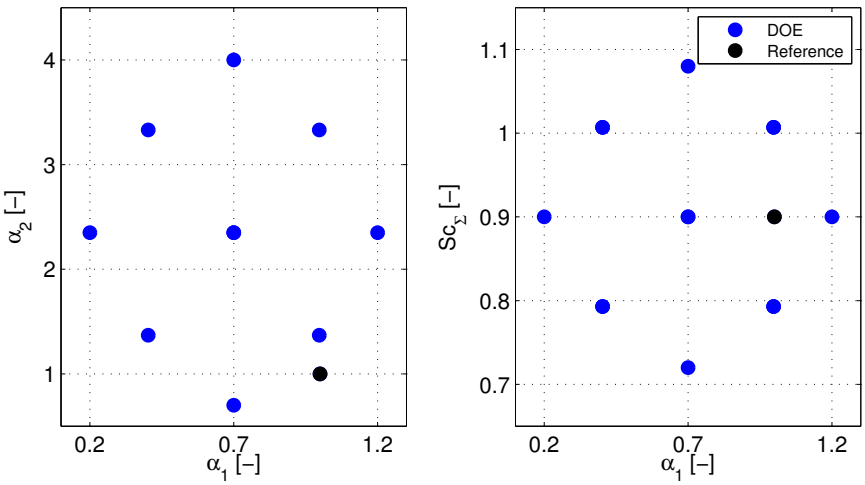

Figure 9: Combinations of input parameters for the optimization DOE. Reference values (black point), DOE simulations (blue point)

Table 6: Ranges for the input factors for the optimization Stage DOE of 3 parameters

	α_1[-]	α_2[-]	Sc_Σ[-]
Reference value	1.0	1.0	0.9
Minimum value	0.2 [*]	0.7 [*]	0.72
Maximum value	1.2	4.0 [**]	1.08
[*] Beheshti et al.[4], [**] Wang et al.[54]			

maximum and minimum values found in the literature are used; or if they are not present, a 20% variation from the reference point is considered (see Table 6). Finally, in Fig. 9 the three parameters included in the DOE design are compared to those of the reference modeling set-up in a two by two combination plot.

Using the results from the 15 simulations of the DOE test plan, the mean error between the measurements along the axis and the calculated SMDs are computed. Then, a mathematical model is constructed by means of a fit to correlate the SMD error output of the 15 simulations conducted. This model

takes the form shown below:

$$\begin{aligned} Output1 = {} & C_1 + C_2 * \alpha_1 + C_3 * \alpha_2 + C_4 * Sc_\Sigma + C_5 * \alpha_1^2 + C_6 * \alpha_2^2 \\ & + C_7 * Sc_\Sigma^2 + C_8 * \alpha_1 * \alpha_2 + C_9 * \alpha_2 * Sc_\Sigma \\ & + C_{10} * \alpha_1^3 + C_{11} * \alpha_2^3 + C_{12} * Sc_\Sigma^3 \end{aligned} \tag{19}$$

where the inputs α_1, α_2 and Sc_Σ are calculated as the following example:

$$\alpha_1 = \big(\alpha_{1value} - (\alpha_{1max} + \alpha_{1min})/2\big)/\big((\alpha_{1max} - \alpha_{1min})/2\big) \tag{20}$$

being α_{1value} the value of α_1 parameter of Σ equation that is used in each simulation of DOE test plan [6], α_{1max} and α_{1min} the maximum and minimum values respectively of α_1 in the range used for the optimization (Table 6).

The mathematical model have been established with 95% confidence, keeping only the significant terms. The coefficients C_1 to C_{12} are described in Table 7 for both optimizations. The fit of this surface compared to the original data is shown by the R^2 value of 0.9924 (HP Optimization) and 0.99 (MP Optimization), which confirm that the mathematical models can predict the response accurately with low prediction error.

Finally, in order to find the optimum parameters, a discretization of 101 points between ranges for each parameter is considered and the 1030301 different combinations are evaluated with the mathematical model. At the end, the minimum error output is found with the constant values, shown in Table 8. The optimum combinations of parameters should be tested under different operating conditions, these results appear on Section 6.2.3, but previously, from the RSM results some trends can be highlighted (apart from the same optimum value for the Sc_Σ parameter).

Table 7: RSM coefficients for each optimization

Coefficient	HP Optimization	MP Optimization
C_1	69.487	13.961
C_2	-36.721	-12.224
C_3	67.117	-6.276
C_4	-1.662	-0.968
C_5	5.228	49.758
C_6	42.458	45.323
C_7	4.918	1.623
C_8	-5.738	-8.015
C_9	1.877	-1.001
C_{10}	36.631	-24.286
C_{11}	-21.177	2.321
C_{12}	7.382	1.603

Table 8: Optimum values of the modeling constants

Constant	α_1[-]	α_2[-]	Sc_Σ[-]
HP Optimization	0.96	1.459	0.9468
MP Optimization	0.77	2.482	0.9468

In Fig. 10 and Fig. 11, the effects of each modeling constant on the error output are shown respectively for each optimization. Additionally to the complete surface obtained with the RSM results, the error of the reference CFD configuration and the optimum values combination are included as well as the tendency expected by the error while changing only one parameter (red line). This line represents a parametric variation of each constant value while keeping fixed the other two to the mean value of the ranges depicted in Table 6, i.e. $\alpha_1 = 0.7$, $\alpha_2 = 2.35$ and $Sc_\Sigma = 0.9$.

Optimization at high pressure injection (HP)

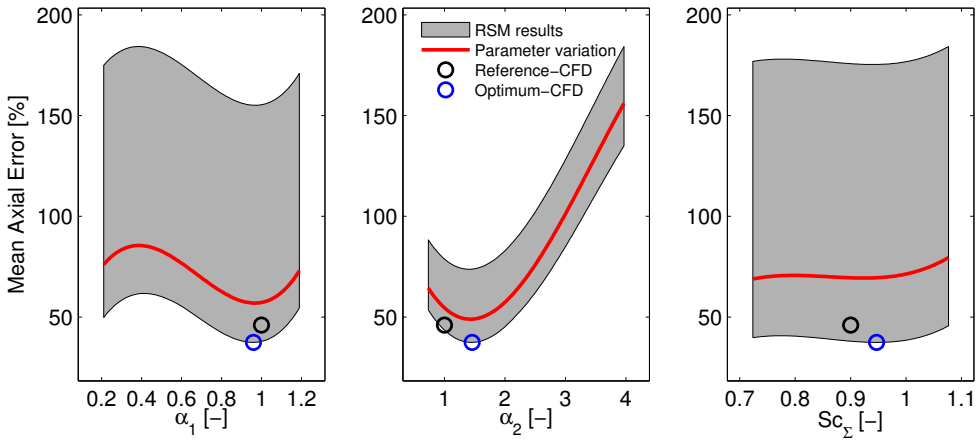

Figure 10: Effect of each input parameter on the mean axial error between SMD model predictions and measurements. Optimum value (blue circle), reference value (black circle), parameter variation (red line). HP Optimization

Results from the first response surface provide really interesting conclusions. The first parameter, α_1, shows a sinusoidal pattern presenting the minimum value in the vicinity of 1. The impact of the second constant, α_2, is really clear. It can be seen how increasing its value above 2, the error is hugely increased as a consequence of too much coalescence. Finally, the Sc_Σ

used in the interphase surface density equation, produces an almost negligible effect on the error as long as its value is below 1, slightly increasing the error on the contrary.

Optimization at medium pressure injection (MP)

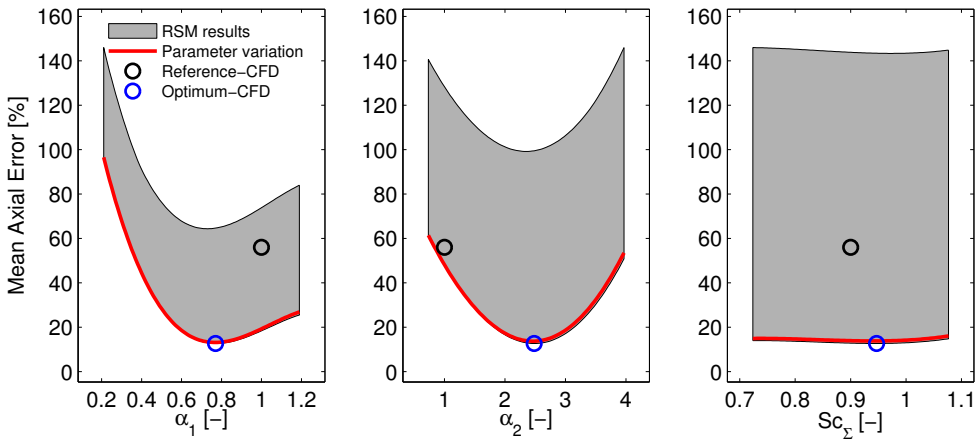

Figure 11: Effect of each input parameter on the mean axial error between SMD model predictions and measurements. Optimum value (blue circle), reference value (black circle), parameter variation (red line). MP Optimization

Regarding the second response surface, first note that due to the mean value of the modeling parameters ranges is quite close to the optimums, the parametric variation line is located at the bottom of the error surface. A completely negligible impact of the Sc_Σ on the error is found. However, results for the other constants are different in comparison with previous optimization. The first parameter, α_1, presents a well defined minimum in the vicinity of 0.8, hugely increasing the error when it takes values below 0.6. Finally, the effect of the second constant, α_2, follows a quadratic function and as a result, the minimum value occurs at its vertex. Moreover, it should

be noted that the predicted mean axial error is more than twice lower to the one achieved with the first optimization (around 16% against 37%).

6.2.2. Validation of optimum parameters

Both optimum sets of model constants values are validated for the corresponding operating condition in Fig. 12, optimization HP at the left, for the spray A baseline condition, and optimization MP at the right, for the case with injection pressure of 100 MPa. Additionally, modeling predictions for the reference set of model constants values are depicted in order to check the real improvement.

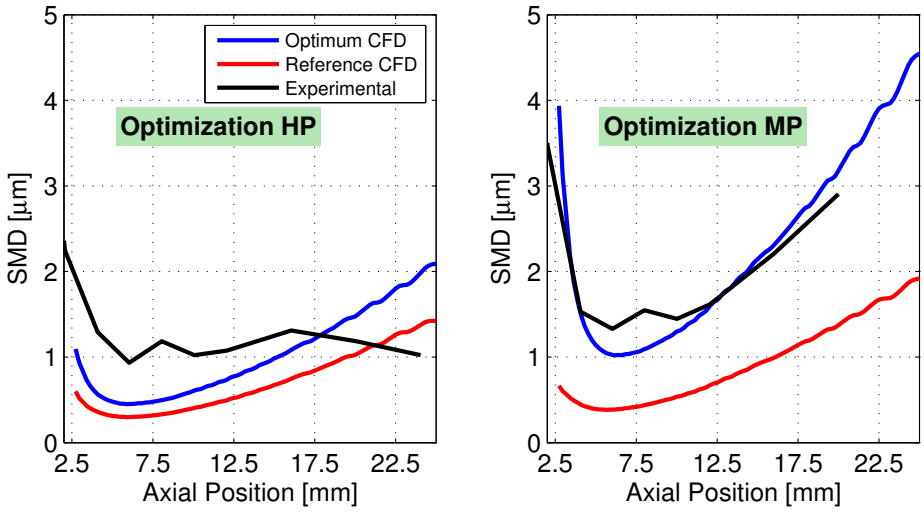

Figure 12: Computed (optimum-blue line and reference-red line) and measured (black line) SMD profiles at the studied conditions

In view of the results, both optimizations improve the performance achieved by the reference set of values. However, in optimization HP the natural trend of model predictions, i.e. increasing droplet diameter due to coalescence downstream, drives the optimal solution to a compromise. Thus, at the

beginning the atomization is more pronounced while from 17.5 *mm* downstream, the coalescence makes SMD predictions greater than measurements. On the other hand, optimization MP performance is remarkably impressive reproducing the experimental trend overall and providing an important improvement with respect to reference set-up predictions. As a result, this second set of optimum parameters, in more agreement with the experimental data, seems to be the suitable set of optimum values for the interphase surface density equation. Nevertheless, modeling performance with these parameters has to be evaluated for the different pressure and ambient conditions before their final selection as the optimum values.

6.2.3. Parametric studies

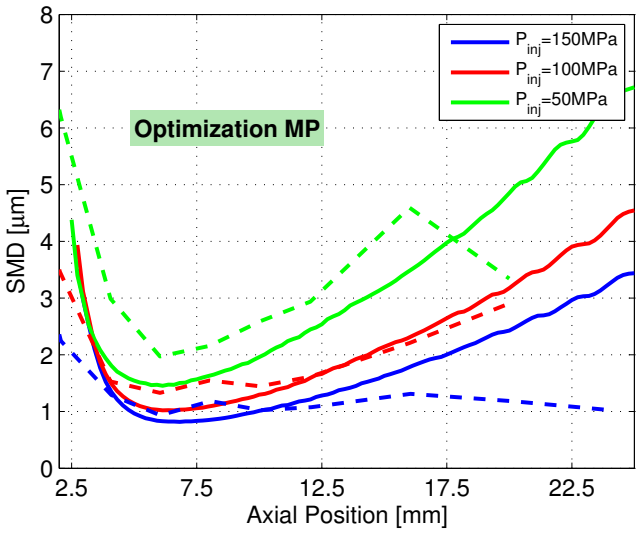

Figure 13: Computed (solid lines) and measured (dashed lines) SMD profiles for different injection pressures

In Figure 13 the influence of injection pressure is shown for the chosen set of constant values. Experimental trends are well reproduced, increased

injection pressure decreases the droplet size, as well as the location at which the minimum droplet size occurs, with little changes with injection pressure. Predictions of this set of optimum parameters are remarkably close to the experimental data, neglecting the coalescence discrepancy for $P_{inj} = 150\ MPa$, condition for which measurements show an unusual and isolate behaviour with axial distance. Moreover, the decrease of droplet size, especially in the regions nearest the nozzle exit, is more enhanced providing a clear distinction among the three injection pressures, in line with observations.

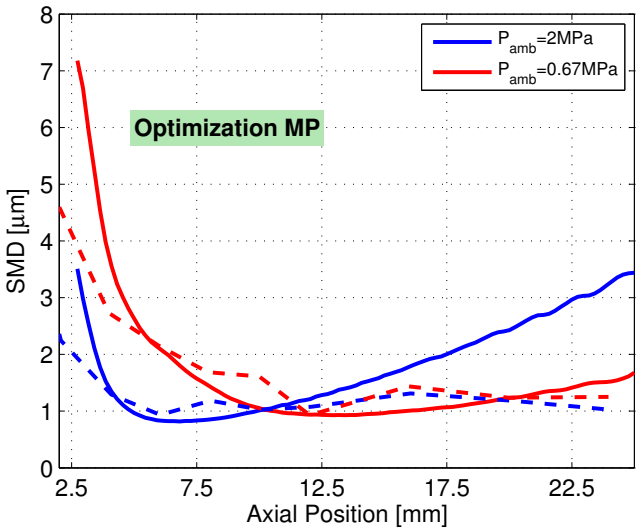

Figure 14: Computed (solid lines) and measured (dashed lines) SMD profiles for different back pressures

Finally, the influence of the back pressure, i.e. ambient density, is shown in Figure 14. Experimental trends are well reproduced, decreased back pressure shows a lower atomization rate of the droplet size, as well as the position at which the minimum droplet size occurs, located further downstream of the nozzle exit, is well captured. In comparison with the baseline condition, in

the case of the lowest back pressure, the increasing droplet size effect with the axial distance is minimized and predictions reach an almost constant SMD value. These quite great predictions confirm that the chosen set of values for the interphase surface density equation are the good ones.

Additionally, in order to evaluate modeling performance separately of ambient density, i.e. air entrainment is changed because of different densities, the results are normalized in Figure 15 with the equivalent diameter, which takes the values of 0.5 for the baseline condition and 0.869 for the reduced back pressure case:

$$d_{eq} = D_o \sqrt{\frac{\rho_f}{\rho_{amb}}}$$

In view of the results, almost an equal minimum SMD prediction is reached in both simulated conditions and the same axial increase due to coalescence is depicted. Thus, it is confirmed that modeling atomization is a consequence of air entrainment.

Summarizing, overall the optimimum set of constants provide good predictions in comparison with the experimental measurements. However, it is still possible to identify some deviations, e.g. an over-predicted coalescence phenomena. This indicates that some improvement of the density surface model should be made in order to overcome it. A different equilibrium surface density (Σ_{eq}) term could improve the results as well as the adoption of a large eddy simulation (LES) treatment of the turbulence modeling.

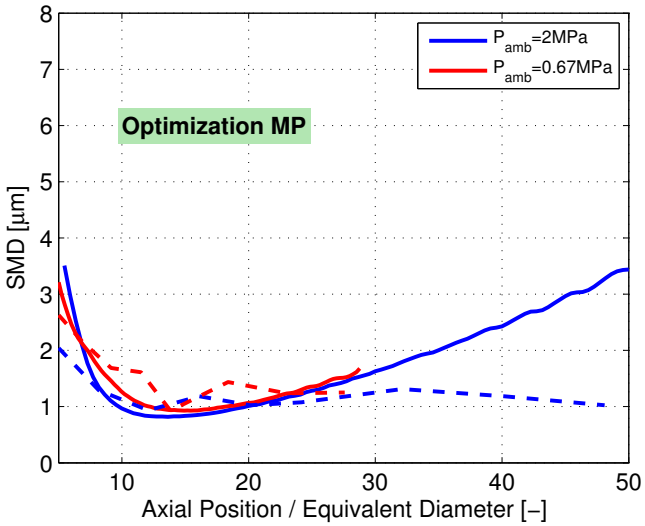

Figure 15: Computed (solid lines) and measured (dashed lines) SMD normalized profiles for different back pressures

7. Summary and Conclusions

The Σ-Y Eulerian atomization model has been applied to the study of direct injection diesel sprays, with a focus on reproducing the internal structure of a diesel spray. Calculations have been validated against x-ray radiography measurements of non-evaporating Spray A condition of ECN, conducted at Argonne National Laboratory, for both the large and small scales of the flow.

First of all, different turbulence models have been evaluated. Predictions made by the standard k-ε model with the corrected value of the $C_{1\epsilon}$ constant, the RNG k-ε model and the SST k-ω model were compared. Only the k-ε turbulence model makes fairly accurate predictions while the other two over-predict the radial dispersion. It has been also proved to be the best turbulence model for external flow application in the near nozzle region, while showing a great performance in internal nozzle flow development, reproduc-

ing the value of the dimensionless coefficients fairly well and with similar accuracy as the other tested models. As a result, this model was selected for all the subsequent calculations.

Moreover, a calibration process of the Σ equation constants has been conducted in order to optimize the primary break-up modeling capabilities. This has been made by means of a Design of Experiments (DOE) technique, known as Response Surface Method (RSM) and comparison with SMD measurements. Apart from optimum values, this methodology is able to point out some interesting cause/effect relations between the input and the output parameters, as the fact that the Schmidt number (Sc_Σ) value used in the diffusion coefficient of the Σ equation presents a negligible effect on the predictions. At the end, a great improvement in modeling performance is achieved in comparison with the reference set-up, and different injection and back pressures conditions are well reproduced proving the great overall effectiveness of the achieved configuration. Nonetheless, the observed deviations with respect to the experimental measurements could indicate that some development of the density surface model should be made, providing an open topic research area in the field of diesel spray atomization processes.

Acknowledgement

Authors acknowledge that part of this work was possible thanks to the Programa de Ayudas de Investigación y Desarrollo (PAID-2013 3198) of the Universitat Politècnica de València. Also this study was partially funded by the Spanish Ministry of Economy and Competitiveness in the frame of the COMEFF(TRA2014-59483-R) project.

References

[1] Atmanl, A., Yksel, B., leri, E., and Karaoglan, A. D., Response surface methodology based optimization of dieseln-butanol cotton oil ternary blend ratios to improve engine performance and exhaust emission characteristics, *Energy Conversion and Management*, vol. **90**, pp. 383 – 394, 2015.

[2] Beale, J. and Reitz, R., Modeling spray atomization with the kelvin-helmholtz/rayleigh-taylor hybrid model, *Atomization and Sprays*, vol. **9**, no. 6, pp. 623–650, 1999.

[3] Beau, P., Funk, M., Lebas, R., and Demoulin, F., Applying quasi-multiphase model to simulate atomization processes in diesel engines: Modeling of the slip velocity, *SAE Technical Paper 2005-01-0220*, 2005.

[4] Beheshti, N., Burluka, A., and Fairweather, M., Assessment of $\Sigma-Y$ liq model predictions for air-assisted atomisation, *Theoretical and Computational Fluid Dynamics*, vol. **21**, no. 5, pp. 381–397, 2007.

[5] Belhadef, A., Vallet, A., Amielh, M., and Anselmet, F., Pressure-swirl atomization: Modeling and experimental approaches, *International Journal of Multiphase Flow*, vol. **39**, pp. 13 – 20, 2012.

[6] Benajes, J., Novella, R., Pastor, J. M., Hernández-López, A., Hasegawa, M., Tsuji, N., Emi, M., Uehara, I., Martorell, J., and Alonso, M., Optimization of the combustion system of a medium duty direct injection diesel engine by combining CFD modeling with experimental validation, *Energy Conversion and Management*, vol. **110**, pp. 212 – 229, 2016.

[7] Blokkeel, G., Barbeau, B., and Borghi, R., A 3D Eulerian model to improve the primary breakup of atomizing jet, *SAE Technical Paper 2003-01-005*, 2003.

[8] Candel, S. and Poinsot, T., Flame stretch and the balance equation for the flame area, *Combustion Science and Technology*, vol. **70**, no. 1-3, pp. 1–15, 1990.

[9] Delhaye, J., Giot, M., and Riethmuller, M., *Thermohydraulics of two-phase systems for industrial design and nuclear engineering*, Series in thermal and fluids engineering, Hemisphere Pub. Corp., 1981.

[10] Demoulin, F., Beau, P., Blokkeel, G., Mura, A., and Borghi, R., A new model for turbulent flows with large density fluctuations: application to liquid atomization, *Atomization and Sprays*, vol. **17**, pp. 315–345, 2007.

[11] Demoulin, F.-X., Reveillon, J., Duret, B., Bouali, Z., Desjonqueres, P., and Menard, T., Toward using direct numerical simulation to improve primary break-up modeling, *Atomization and Sprays*, vol. **23**, no. 11, pp. 957–980, 2013.

[12] Desantes, J., García, J., Pastor, J., and Pandal, A., A comparison of diesel sprays CFD modelling approaches: DDM vs $\Sigma - Y$ eulerian atomization model, *Atomization and Sprays*, vol. **26**, pp. 713–737, 2016.

[13] Desantes, J., García-Oliver, J., Pastor, J., Pandal, A., Baldwin, E., and Schmidt, D., Coupled/decoupled spray simulation comparison of the ECN spray a condition with the $\Sigma - Y$ eulerian atomization model, *International Journal of Multiphase Flow*, vol. **80**, pp. 89 – 99, 2016.

[14] Desantes, J., Salvador, F., López, J., and De la Morena, J., Study of mass and momentum transfer in diesel sprays based on x-ray mass distribution measurements and on a theoretical derivation, *Experiments in Fluids*, vol. **50**, no. 2, pp. 233–246, 2011.

[15] Dukowicz, J., A particle fluid numerical model for liquid sprays, *Journal of Computational Physics*, vol. **2**, pp. 111–566, 1980.

[16] ECN, Engine combustion network data archive, 2012.
URL `http://www.sandia.gov/ecn/`

[17] ECN, LVF data archive, 2014.
URL `http://www.sandia.gov/ecn/argonne/assets/datafiles/mixture/rad675.php`

[18] García-Oliver, J., Pastor, J., Pandal, A., Trask, N., Baldwin, E., and Schmidt, D., Diesel spray CFD simulations based on the $\Sigma - Y$ eulerian atomization model, *Atomization and Sprays*, vol. **23**, pp. 71–95, 2013.

[19] Hatami, M., Cuijpers, M., and Boot, M., Experimental optimization of the vanes geometry for a variable geometry turbocharger (vgt) using a design of experiment (doe) approach, *Energy Conversion and Management*, vol. **106**, pp. 1057 – 1070, 2015.

[20] Ishii, M., *Thermofluid Dynamics of Two-phase Flows*, Eyrolles, Paris, France, 1975.

[21] Kastengren, A., Ilavsky, J., Viera, J. P., Payri, R., Duke, D., Swantek, A., Tilocco, F. Z., Sovis, N., and Powell, C., Measurements of droplet size in shear-driven atomization using ultra-small angle x-ray scattering, *International Journal of Multiphase Flow*, vol. **92**, pp. 131 – 139, 2017.

[22] Kastengren, A., Tilocco, F. Z., Powell, C. F., Manin, J., Pickett, L. M., Payri, R., and Bazyn, T., Engine combustion network (ECN):measurements of nozzle geometry and hydraulic behavior, *Atomization and Sprays*, vol. **22**, pp. 1011–1052, 2012.

[23] Kastengren, A. L., Powell, C. F., Wang, Y., Im, K.-S., and Wang, J., X-ray radiography measurements of diesel spray structure at engine-like ambient density, *Atomization and Sprays*, vol. **19**, no. 11, pp. 1031–1044, 2009.

[24] Kastengren, A. L., Tilocco, F. Z., Duke, D. J., Powell, C. F., Seoksu, M., and Xusheng, Z., Time-resolved x-ray radiography of diesel injectors from the engine combustion network, *ICLASS Paper*, no. 1369, 2012.

[25] Lebas, R., Menard, T., Beau, P., Berlemont, A., and Demoulin, F., Numerical simulation of primary break-up and atomization: DNS and modeling study, *International Journal of Multiphase Flow*, vol. **35**, pp. 247–260, 2009.

[26] Lee, C. H. and Reitz, R. D., CFD simulations of diesel spray tip penetration with multiple injections and with engine compression ratios up to 100:1, *Fuel*, vol. **111**, no. 0, pp. 289 – 297, 2013.

[27] Lucchini, T., D'Ericco, G., and Ettorre, D., Numerical investigation of the spray-mesh-turbulence interactions for high-pressure, evaporating sprays at engine conditions, *International Journal of Heat and Fluid Flow*, vol. **32**, pp. 285–297, 2011.

[28] Macián, V., Bermúdez, V., Payri, R., and Gimeno, J., New technique for determination of internal geometry of a diesel nozzles with the use of silicone methodology, *Experimental Techniques*, vol. **37**, pp. 39–43, 2003.

[29] Marble, F. and Broadwell, J., *The Coherent Flame Model for Turbulence Chemical Reactions*, Technical report, Project Squid Headquarters. Chaffee Hall, Purdue University, West Lafayette, Indiana, 1977.

[30] Myers, R. H., Montgomery, D. C., and Anderson-Cook, C. M., *Response Surface Methodology: Process and Product Optimization Using Designed Experiments*, 3rd Edition, Wiley, 2015.

[31] Naber, J. and Siebers, D., Effects of gas density and vaporization on penetration and dispersion of diesel sprays, *SAE Technical Paper*, no. 960034, 1996.

[32] Navarro-Martinez, S., Large eddy simulation of spray atomization with a probability density function method, *International Journal of Multiphase Flow*, vol. **63**, pp. 11 – 22, 2014.

[33] Payri, F., Payri, R., Salvador, F., and Martnez-Lpez, J., A contribution to the understanding of cavitation effects in diesel injector nozzles through a combined experimental and computational investigation, *Computers & Fluids*, vol. **58**, pp. 88 – 101, 2012.

[34] Payri, R., García, J., Salvador, F., and Gimeno, J., Using spray momentum flux measurements to understand the influence of diesel nozzle geometry on spray characteristics, *Fuel*, vol. **84**, no. 5, pp. 551 – 561, 2005.

[35] Payri, R., Salvador, F., Gimeno, J., and de la Morena, J., Effects of nozzle geometry on direct injection diesel engine combustion process, *Applied Thermal Engineering*, vol. **29**, no. 10, pp. 2051 – 2060, 2009.

[36] Payri, R., Salvador, F., Gimeno, J., and Zapata, L., Diesel nozzle geometry influence on spray liquid-phase fuel penetration in evaporative conditions, *Fuel*, vol. **87**, no. 7, pp. 1165 – 1176, 2008.

[37] Perini, F., Miles, P. C., and Reitz, R. D., A comprehensive modeling study of in-cylinder fluid flows in a high-swirl, light-duty optical diesel engine, *Computers & Fluids*, vol. **105**, pp. 113 – 124, 2014.

[38] Pickett, L., Manin, J., Kastengren, A., and Powell, C., Comparison of near-field structure and growth of a diesel spray using light-based optical microscopy and x-ray radiography, *SAE Int. J. Engines*, vol. **7**, no. 2, 2014.

[39] Pope, S., An explanation of the turbulent round-jet/plane-jet anomaly, *AIAA*, vol. **16**, pp. 279–281, 1978.

[40] Reid, R., Prausnitz, J., and Poling, B., *The Properties of Gases and Liquids*, McGraw-Hill, 1987.

[41] Salvador, F., Carreres, M., Jaramillo, D., and Martínez-López, J., Analysis of the combined effect of hydrogrinding process and inclination angle on hydraulic performance of diesel injection nozzles, *Energy Conversion and Management*, vol. **105**, pp. 1352 – 1365, 2015.

[42] Salvador, F., Carreres, M., Jaramillo, D., and Martínez-López, J., Comparison of microsac and VCO diesel injector nozzles in terms of internal nozzle flow characteristics, *Energy Conversion and Management*, vol. **103**, pp. 284 – 299, 2015.

[43] Salvador, F., Gimeno, J., Pastor, J., and Martí-Aldaraví, P., Effect of turbulence model and inlet boundary condition on the diesel spray behavior simulated by an eulerian spray atomization (ESA) model, *International Journal of Multiphase Flow*, vol. **65**, pp. 108–116, 2014.

[44] Siebers, D., Liquid-phase fuel penetration in diesel sprays, *Trans. SAE*, vol. **107**, pp. 1205–1227, 1998.

[45] Siebers, D., Liquid-phase fuel penetration in diesel sprays based on mixing-limited vaporization, *Trans. SAE*, vol. **108**, pp. 703–728, 1999.

[46] Siebers, D. L., 2008. Recent developments on diesel fuel jets under quiescent conditions, *Flow and combustion in reciprocating engines*. Arcoumanis, C. and Kamimoto, T. (Eds.). Springer-Verlag, Berlin, pp. 257–308.

[47] Silva, V. and Rouboa, A., Combining a 2-d multiphase CFD model with a response surface methodology to optimize the gasification of portuguese biomasses, *Energy Conversion and Management*, vol. **99**, pp. 28 – 40, 2015.

[48] Som, S., Longman, D., Ramírez, A., and Aggarwal, S., A comparison of injector flow and spray characteristics of biodiesel with petrodiesel, *Fuel*, vol. **89**, no. 12, pp. 4014 – 4024, 2010.

[49] Trask, N., Schmidt, D., Lightfoot, M., and Danczyk, S., Compressible modeling of the internal flow in a gas-centered swirl-coaxial fuel injector, *Journal of Propulsion and Power*, vol. **28(4)**, pp. 685–693, 2012.

[50] Vallet, A. and Borghi, R., Modélisation Eulerienne de l'atomisation d'un jet liquide, *C.R. Acad. Sci, Paris*, vol. **327**, pp. 1015–1020, 1999.

[51] Vallet, A., Burluka, A., and Borghi, R., Development of a Eulerian model for the "atomization" of a liquid jet, *Atomization and Sprays*, vol. **11**, pp. 619–642, 2001.

[52] Vujanovi, M., Petranovi, Z., Edelbauer, W., Baleta, J., and Dui, N., Numerical modelling of diesel spray using the eulerian multiphase approach, *Energy Conversion and Management*, vol. **104**, pp. 160 – 169, 2015, special Issue on Sustainable development of energy, water and environment systems.

[53] Wang, Y., Grover, R., Schmidt, D., Diwakar, R., and Kuo, T.-W., Application of interface area density modeling to define spray plume boundary, *ILASS Paper*, 2015.

[54] Wang, Y., Lee, W., Reitz, R., and Diwakar, R., Numerical simulation of diesel sprays using an eulerian-lagrangian spray and atomization (ELSA) model coupled with nozzle flow, *SAE Technical Paper 2011-01-0386*, 2011.

[55] Weller, H., Tabor, G., Jasak, H., and Fureby, C., A tensorial approach to computational continuum mechanics using object-oriented techniques, *Computers in Physics*, vol. **12**, pp. 620–631, 1998.

[56] Xue, Q., Battistoni, M., Powell, C., Longman, D., Quan, S., Pomraning, E., Senecal, P., Schmidt, D., and Som, S., An eulerian CFD model and x-ray radiography for coupled nozzle flow and spray in internal combustion engines, *International Journal of Multiphase Flow*, vol. **70**, no. 0, pp. 77 – 88, 2015.

[57] Xue, Q. and Kong, S.-C., Development of adaptive mesh refinement scheme for engine spray simulations, *Computers & Fluids*, vol. **38**, no. 4, pp. 939 – 949, 2009.